# Bed Expansion of Liquid-Solid Inverse Fluidization

**D. G. Karamanev and L. N. Nikolov**
Biological Faculty, Sofia University, 1421 Sofia, Bulgaria

*The bed expansion characteristics of two-phase inverse fluidization were studied. Twelve different spheres with diameters from 1.31 to 7.24 mm and densities between 75 and 930 kg/m$^3$ were fluidized with water. The experimental $\ln\epsilon$-$\ln U$ curves were parallel to those predicted by the model of Richardson and Zaki and therefore the exponents n were similar. However, $U_i$, the liquid velocity at $\epsilon = 1$ differed from that predicted from the standard drag curve for $Re_t > 130$. This can be explained by the fact that the drag curve of a freely rising light sphere differs from that of a falling particle. The values of $U_i$ calculated using this modified drag curve were in good agreement with the experimental results. The difference between experimental and calculated from the Ergun equation minimal fluidization velocities is explained by the difference in mechanical inertia of the light and heavy particles.*

## Introduction

The term "fluidization" is usually associated with two- or three-phase systems, in which solid particles are fluidized by a liquid or gas stream flowing in the direction opposite to that of gravity. In this classic case of fluidized systems the solid particles have a higher density than the fluid. When the bed solids have a density lower than that of the fluid (usually liquid), the bed can be fluidized by a downflow of this liquid (Muroyama and Fan, 1985). This multiphase system is called inverse fluidized bed. The first studies on the application, hydrodynamics and mass transfer of two-phase inverse fluidization were performed in last few years (Nikolov et al., 1981; Fan et al., 1982; Garnier et al., 1990; Nikov and Karamanev, 1991). Inverse fluidization is used in biotechnology as the basis of a new type of bioreactor, the so-called inverse fluidized bed biofilm reactor.

In the last decade the application of fluidization technique in biotechnology or biofluidization became one of the most important areas in bioreactor engineering (Shugerl, 1989; Atkinson, 1981). The upflow fluidized bed bioreactors are among the most efficient apparatuses for aerobic and anaerobic wastewater treatment (Jeris et al., 1981; Jewell et al., 1981), penicillin production (Oh et al., 1988; Endo et al., 1988), and phenol degradation (Holladay et al., 1978; Tang and Fan, 1987; Livingston and Chase, 1989). However, the important problem of biofilm thickness control is the main reason for the limited industrial application of these systems. The control of biofilm thickness within a narrow range is achieved in the inverse fluidized bed biofilm reactor. It was found that this bioreactor is very efficient when used for biological aerobic wastewater treatment both under laboratory conditions and when scaled up (Nikolov and Karamanev, 1987; Nikolov et al., 1990). Another important biotechnological process, ferrous iron oxidation by *Thiobacillus ferrooxidans*, was also carried out with very high efficiency in an inverse fluidized bed biofilm reactor (Nikolov and Karamanev, 1987; Karamanev and Nikolov, 1988). This bioreactor was successfully used for milk protein hydrolysis by *Lactobacillus helveticus* (Dion et al., 1988). Moreover, this apparatus was found to be suitable as a laboratory tool for biofilm processes research (Nikolov and Karamanev, 1990). Mathematical modelling of the inverse fluidized bed biofilm reactor requires knowledge of the hydrodynamics of inverse fluidization (Chavarie et al., 1985; Chavarie and Karamanev, 1986). Unfortunately, the latter has not been studied enough. Only two articles on the hydrodynamics of two-phase inverse fluidization have been published (Fan et al., 1982; Garnier et al., 1990). Two mathematical models relating bed expansion to liquid velocity were proposed by Fan et al. (1982). These models were based on experimental data obtained from expansion of beds containing solid particles with densities from 822 to 930 kg/m$^3$ and only one bed with lighter particles with a density of 388 kg/m$^3$. The latter bed however was expanded only within a narrow range of $\epsilon$, between 0.39 and 0.54. Particle

Correspondence concerning this article should be addressed to D. G. Karamanev presently at the Department of Chemical Engineering, Ecole Polytechnique de Montreal, P.B. 6079, St. "A", Montreal, Canada H3C 3A7.

sizes were between 4.76 and 19.1 mm, corresponding to $d/D$ ratios from 0.062 to 0.250, respectively. The Archimedes number varied between $1.1\times10^5$ and $7.65\times10^6$. Particles in the inverse fluidized bed biofilm reactor usually have diameters of 1 to 5 mm, densities between 200 and 990 kg/m$^3$ and $d/D$ ratio between 0.001 and 0.1. Recently, preliminary data have shown that fluidized particles with densities between 100 and 200 kg/m$^3$ have unusual expansion characteristics—lower than the expected minimum and maximum fluidization velocities (Nikolov and Karamanev, 1991).

Therefore, the main aim of this work was to investigate the hydrodynamics of a two-phase inverse fluidized bed containing solid particles with a large range of diameters, densities and, therefore, Archimedes numbers. The applicability of the standard drag curve to the case of freely rising light particles was examined. A mathematical model of bed expansion as a function of liquid velocity was developed.

Since mathematical models were used for the prediction of the inverse fluidized bed expansion, a short literature survey of bed expansion correlations will be made.

## *Mathematical models of bed expansion*

The different models for correlation of bed expansion with superficial fluid velocity can be classified into three main groups (Fan et al., 1982). The first group is based on correlations giving the dependence between $U/U_i$ and $\epsilon$. The Richardson and Zaki (1954) model is most popular in this group. In the second group of models the drag function for multiparticle system is used. It is usually given as a function of $Re$ and $Ar$. The models of Ramamurthy and Subbaraju (1973) and Riba and Couderc (1977) are typical for this group. The third group of models is based on the dependence between $\epsilon$ and the main variables of the fluidized bed as in the Wen and Yu (1966) correlation.

Among all these correlations, the Richardson and Zaki model is probably the most popular one due to its simplicity and its good agreement with experimental data. It is based on the following equation:

$$\frac{U}{U_i}=\epsilon^n \tag{1}$$

where the exponent $n$ can be determined from the correlations:

$$n=\left(4.4+18\,\frac{d}{D}\right)Re_t^{-0.1} \tag{1a}$$

for $1<Re_t<200$

$$n=4.4Re_t^{-0.1} \tag{1b}$$

for $200<Re_t<500$ and

$$n=2.4 \tag{1c}$$

for $Re_t>500$.

$U_i$, the superficial fluid velocity at $\epsilon=1$, can be calculated from the following equation (Richardson, 1971):

$$\log U_i=\log U_t-\frac{d}{D} \tag{2}$$

where $U_t$ is the particle terminal velocity as given by the following equation (Den, 1980):

$$U_t=\sqrt{\frac{4(\rho_p-\rho_l)gd}{3\rho_l C_D}} \tag{3}$$

where the drag coefficient $C_D$ is determined from the standard drag curve—the dependence $\ln C_D-\ln Re_t$ (Den, 1980).

The equation below based on a correlation of the standard drag curve in the range $12.2<Re_t<6{,}350$ can be used for calculating the particle terminal velocity (Clift et al., 1978):

$$\log Re_t=-1.814+1.347\log N_D-0.1243(\log N_D)^2+0.00634(\log N_D)^3 \tag{4}$$

where $N_D$, the so called Best number, is defined as:

$$N_D=C_D Re_t^2=\frac{4\rho_l(\rho_p-\rho_l)gd^3}{3\mu^2}=\frac{4}{3}\,Ar \tag{5}$$

The standard drag curve is based on experimental data with settling in a fluid heavy spherical particles when $\rho_p>\rho_l$. There is no information available if for the validity of the standard drag curve in the case of freely rising light spheres with $\rho_p<\rho_l$. Nevertheless, in many publications, including one of the best monographs on particle-fluid interactions (Clift et al., 1978, p. 113), the assumption was made that the drag curves of free falling and rising solid spheres are identical. This assumption was not confirmed by experimental data.

Only two correlations are proposed in the literature for inverse fluidized bed expansion (Fan et al., 1982). The first of them is based on the group I model:

$$\frac{U}{U_i}=\epsilon^n \tag{6}$$

where

$$n=15Re_t^{-0.35}e^{3.9\frac{d}{D}} \tag{6a}$$

for $350<Re<1{,}250$ and

$$n=8.6Re_t^{-0.2}e^{-0.75\frac{d}{D}} \tag{6b}$$

for $Re_t>1{,}250$. The article does not mention how the velocities $U_i$ in this model were determined, but supposedly this has been done using the well-known standard drag curve.

A model based on the drag function for the multiparticle system $f$ (second group) has also been proposed by Fan et al. (1982):

$$f=\frac{Ar}{13.9Re^{1.4}} \tag{7a}$$

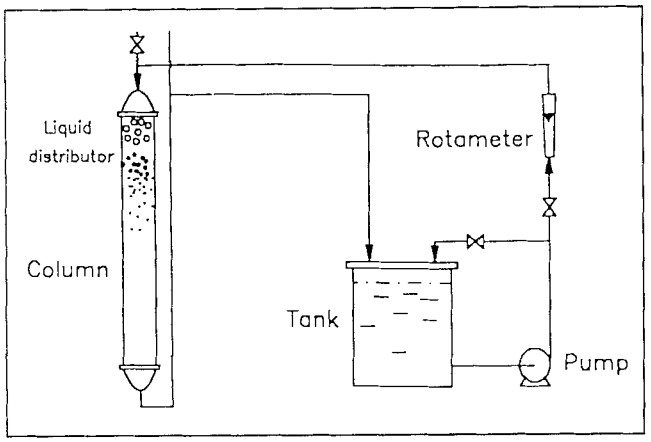


**Figure 1. Experimental unit for bed expansion studies.**

for $2<Re<500$ and

$$f=\frac{3Ar}{Re^2} \tag{7b}$$

for $Re>500$. The drag function $f$ is defined as follows:

$$f=3.21\epsilon^{-4.05}Ar^{-0.07}e^{3.5\frac{d}{D}} \tag{8}$$

The ranges of applicability of Eqs. 6 and 7 concerning $Ar$ and $d/D$ ratio were mentioned earlier.

In the present article the model of Richardson and Zaki will be used since it has been widely used for the description of upflow fluidized bed expansion. The two models of Fan et al. (1982) will also be evaluated as they are only models developed for description of bed expansion in inverse fluidization.

## Materials and Methods

The experimental setup for determining the effect of liquid velocity on inverse fluidized bed expansion is shown in Figure 1. The glass column dimensions were: ID 80 mm, height 1.3 m. The upper part of the column was filled with two beds of solid particles for liquid distribution. A 70 mm high bed of styrofoam particles with average size of 12 mm and density of 70 kg/m$^3$ was placed above the bed (70 mm high) of glass spheres with diameter 3 mm. The latter was supported by a 16-mesh stainless steel grid. A glass stopcock was connected to the highest point of the apparatus for periodical degassing of the liquid.

Tap water was used as a liquid phase. Its flow rate was measured by a calibrated rotameter or determined from the weight of liquid, leaving the column for a certain period of time. A Sartorius Excellence electronic balance (maximum weight 12 kg, accuracy 0.1 g) was used.

Expanded polystyrene (styrofoam) spheres were used as a solid phase. This material is very suitable for this study because it allows the formation of spherical particles with any diameter from 1 to 8 mm and any density from 70 to 1,070 kg/m$^3$. Particles with the desired density were obtained by the following procedure. Nonexpanded polystyrene spheres used as a raw material for styrofoam production with a defined diameter and a density of 1,070 kg/m$^3$ were mixed with boiling water. Their diameter began to increase and therefore the density decreased due to expansion. When the desired density was obtained, further expansion was stopped by adding cold water. The maximum possible expansion of polystyrene corresponds to a density of 70 kg/m$^3$. Styrofoam pores are closed and therefore particle density remains constant when in contact with cold water.

**Table 1. Physical Parameters of the Solid Particles**

| | | $d$ | | $\rho_p$ | | | |
|---|---|---|---|---|---|---|---|
| No. | Material | Mean, mm | 95% Conf. | Mean, kg/m$^3$ | 95% Conf. | $\epsilon_o$ | $d/D$ |
| 1 | Styrofoam | 5.77 | 0.22 | 159 | 13 | — | 0.072 |
| 2 | Styrofoam | 3.46 | 0.048 | 75 | 3.4 | 0.41 | 0.043 |
| 3 | Styrofoam | 2.33 | 0.063 | 314 | 6.2 | 0.40 | 0.029 |
| 4 | Styrofoam | 2.75 | 0.11 | 427 | 37 | 0.41 | 0.035 |
| 5 | Styrofoam | 5.35 | 0.11 | 201 | 16 | 0.41 | 0.067 |
| 6 | Styrofoam | 7.24 | 0.12 | 96 | 4.4 | 0.41 | 0.091 |
| 7 | Styrofoam | 1.55 | 0.064 | 292 | 28 | — | 0.020 |
| 8 | Styrofoam | 2.40 | 0.076 | 155 | — | 0.40 | 0.030 |
| 9 | Styrofoam | 1.31 | 0.078 | 650 | 40 | 0.41 | 0.016 |
| 10 | Styrofoam | 3.16 | — | 705 | — | 0.40 | 0.040 |
| 11 | Styrofoam | 3.03 | — | 854 | — | 0.41 | 0.038 |
| 12 | Polyethylene | 3.57 | — | 930 | — | 0.41 | 0.045 |

Particle density was measured by determining their volume and mass. The volume was measured using a pycnometer filled with distilled water. Temperature was kept between 30.0 and 30.1°C by means of a digital water bath circulator (Haake Co., USA). Particle mass was measured by a Sartorius Supermicro S4 balance with a precision of 1 $\mu$g. The density was calculated by dividing the mass by the volume of each particle. Particle diameters were calculated from their volume or directly measured by a micrometer. The densities and diameters of 20 to 40 particles in each bed were measured. Mean values, standard deviations and 95% confidence intervals of these parameters were calculated. The sphericity of styrofoam particles was estimated from the ratio between the maximum and minimum size of each particle. This ratio did not exceed 1.1 in at least 90% of the particles in each bed and therefore the shape of the particles was assumed to be spherical.

Eleven different styrofoam spheres obtained according to the above procedure were used as fluidized particles. Their average diameters varied from 1.31 to 7.24 mm, corresponding to the $d/D$ values from 0.016 to 0.091. Particle densities were between 75 and 854 kg/m$^3$. Polyethylene particles with a mean diameter of 3.57 mm and density of 930 kg/m$^3$ were also used. The mean diameters and densities of the particles of each bed and the 95% confidence intervals are summarized in Table 1.

The inverse fluidized bed porosity was determined from measurement of the bed height.

## Results

Several specific characteristics of the two-phase inverse fluidized bed usually not observed in "classic" upflow fluidization must be underlined.

The liquid entering the fluidized bed often carries gas bubbles. When a bubble enters an upflow fluidized bed, it leaves the bed rapidly because the direction of its free rise is the same

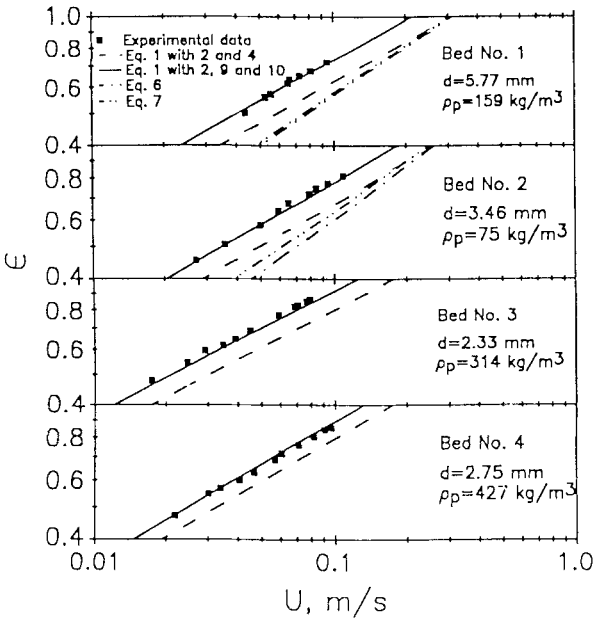


**Figure 2. Dependence between $\ln\epsilon$ and $\ln U$: bed no. 1-4.**

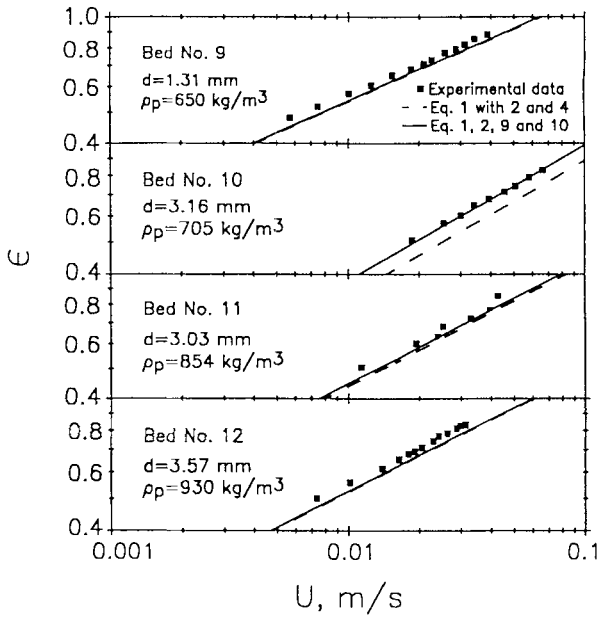


**Figure 4. Dependence between $\ln\epsilon$ and $\ln U$: bed no. 9-12.**

as the direction of liquid flow and therefore it does not change significantly the hydrodynamic state of the bed. In the inverse fluidized bed, these directions are opposite to each other and a bubble entering the bed with the liquid phase usually remains in it, provided that it is not too small. In the latter case the bubble moves downwards together with the liquid. Consequently, since gas bubbles accumulate in the inverse fluidized bed, they affect the hydrodynamic measurements. It is very important therefore to eliminate gas bubbles from the liquid entering the bed. Gas bubbles were removed from the apparatus through the stopcock (Figure 1) before each experimental run.

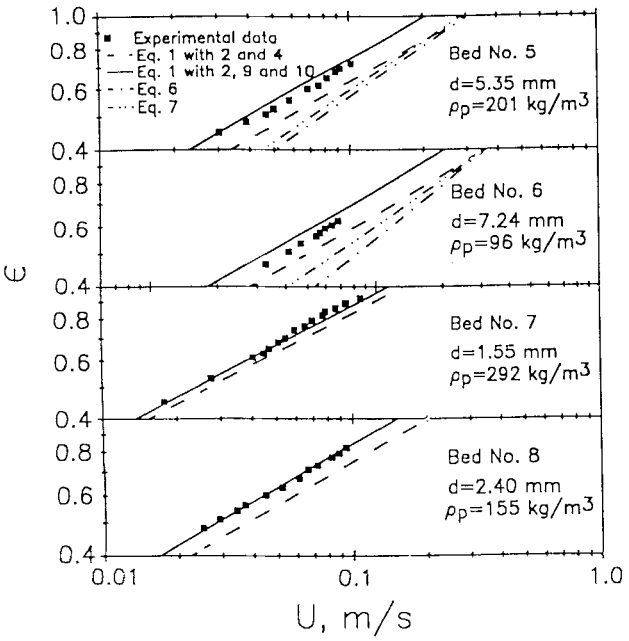


**Figure 3. Dependence between $\ln\epsilon$ and $\ln U$: bed no. 5-8.**

The solid particles used in the upflow fluidized beds are usually of nonporous materials such as glass, metals, and sand. Each of these materials have a certain constant density. The styrofoam spheres used in the inverse fluidized bed are usually not expanded absolutely uniformly and hence there exists a certain distribution of particle density. For more precise study of the bed expansion characteristics, this distribution should be confined to more narrow limits. This was achieved by expanding the bed in such a way that its lower boundary reached the output of the column and heaviest particles were washed out with the liquid. Therefore, the particles with higher density were removed from the bed before the experiments. The particles with smaller density were not separated. The average particle diameters and densities as well as the confidence intervals shown in Table 1 were obtained after the treatment described above.

The experimental results of bed expansion are given in Figures 2-4. It can be seen that the experimental data of each fluidized bed plotted as a function $\ln\epsilon$-$\ln U$ can be interpolated by a straight line. When the Richardson and Zaki correlation is used for modeling of these data, the slope of the lines $\ln\epsilon$-$\ln U$ are equal to $1/n$ and the intercept of these lines with the horizontal axis at $\epsilon = 1$ gives $\ln U_i$ according the following form of Eq. 1: $\ln\epsilon = (1/n)\ln U - (1/n)\ln U_i$. The values of $n$ and $U_i$ calculated by linear regression of the experimental data shown in Figures 1-7 are given in Table 2. The same table shows also the values of $n$ calculated from Eq. 1 and Eq. 6, as well as the values of $U_i$ determined using the standard drag curve (respectively Eq. 4) and Eqs. 2 and 3. The Archimedes number and $Re_t$ are also given in Table 2. $Re_t$ was calculated using the experimental value of $U_t$. The latter was determined from the experimental values of $U_i$ using Eq. 2.

The curves calculated from Eqs. 1, 6 and 7 are also plotted in Figures 2-4.

Table 2. Summary of Experimental Results

| Bed No. | $Ar$ ($\times 10^6$) | $n$ (Exp.) | $n$ (Eq. 1) | $n$ (Eq. 6) | $U_i$ exp. (m/s) | $U_i$ std. drag curve (m/s) | $U_i$ $C_D=0.95$ (m/s) | $Re_t$ ($U_t$ from Eq. 2 and Exp. $U_i$) |
|---|---|---|---|---|---|---|---|---|
| 1 | 1.58 | 2.51 | 2.4 | 1.95 | 0.19 | 0.323 | 0.213 | 1,290 |
| 2 | 0.376 | 2.34 | 2.4 | 1.90 | 0.178 | 0.264 | 0.184 | 680 |
| 3 | 0.108 | 2.54 | 2.50 | ** | 0.120 | 0.176 | 0.128 | 300 |
| 4 | 0.117 | 2.50 | 2.4 | ** | 0.143 | 0.176 | 0.133 | 426 |
| 5 | 1.20 | 2.44 | 2.4 | 1.96 | 0.225 | 0.303 | 0.206 | 1,400 |
| 6 | 3.39 | 2.41 | 2.4 | 1.75 | 0.264 | 0.369 | 0.243 | 2,350 |
| 7 | 0.026 | 2.66 | 2.85 | ** | 0.102 | 0.133 | 0.114 | 165 |
| 8 | 0.115 | 2.59 | 2.41 | ** | 0.159 | 0.202 | 0.152 | 409 |
| 9 | 0.008 | 3.25 | 3.02 | ** | 0.061 | 0.073 | 0.073* | 83 |
| 10 | 0.091 | 2.57 | 2.44 | ** | 0.107 | 0.127 | 0.103 | 370 |
| 11 | 0.040 | 2.71 | 2.53 | ** | 0.076 | 0.084 | 0.079 | 251 |
| 12 | 0.032 | 2.77 | 2.58 | ** | 0.052 | 0.060 | 0.060 | 206 |

*$U_i$ is calculated using the standard drag curve since $Re_t < 130$.
**The values of $Ar$ and $d/D$ are outside the range of applicability of Eq. 6.

## Discussion

### The exponent n

On analyzing the results summarized in Table 2 it can be seen that the exponents $n$ obtained from the experimental data and that calculated from the correlations of Richardson and Zaki (Eqs. 1a-1c) are in good agreement. The differences between them varies from $-6.8$ to $+6.7\%$ with a variation of 5%. Therefore, the experimental and the calculated curves from the Richardson-Zaki model are almost parallel (Figures 2-4). The values for the exponents $n$ calculated from the correlations of Fan et al. (1982) (Eqs. 6a and 6b), however differ from our experimental data by up to 27%.

### The superficial velocity $U_i$

The velocities $U_i$ used in Eqs. 1 and 6 were calculated from the standard drag curve and Eqs. 2, 4 and 5, where the term $(\rho_p - \rho_l)$ was substituted by $(\rho_l - \rho_p)$. Compared to $U_i$ obtained from the intercept of the experimental lines with the axis at $\epsilon = 1$, all calculated velocity values are larger by up to 54% with a variation of 36%. It is interesting to note that the deviation of the calculated from the experimental values of $U_i$ increases as $Re_t$ increases. This coincidence could be explained in three ways. First, the Richardson and Zaki equation is not able to describe adequately the expansion characteristics of the inverse fluidized bed. The second explanation could be that the porosity of the fixed bed of light particles $\epsilon_o$ is not equal to that of the heavy particles. The data in Table 1 however show that this is not the case. The third supposition, which seemed less probable, was that the $U_t$ of a freely rising spherical particle does not obey the laws of a freely settling sphere. Much to our surprise, the last hypothesis was found to be true. After extensive experimental work (Karamanev and Nikolov, 1992), it was found that the standard drag curve is not valid for rising spheres with a density below 300 kg/m$^3$. In this case the drag curve can be described by the following relationships:

$$\log Re_t = -1.814 + 1.347 \log N_D - 0.1243 (\log N_D)^2 + 0.00634 (\log N_D)^3 \quad (9)$$

for $12.2 < Re_t < 130$ and

$$Re_t = \sqrt{\frac{N_D}{0.95}} \quad (10)$$

(or $C_D = 0.95$) for $130 < Re_t < 9 \times 10^4$.

It can be seen that when $Re_t$ is below 130, the drag coefficients of the rising and settling particles are the same, while they differ outside this region. We called this dependence between $C_D$ and $Re_t$ the modified drag curve. When $\rho_p > 900$ kg/m$^3$, the $\ln C_D$-$\ln Re_t$ curve for a freely rising particle follows the curve for a falling particle up to $Re_t$ of 1,500-2,000. The explanation for these findings is given elsewhere (Karamanev and Nikolov, 1992). Using Eqs. 9 and 10 together with Eqs. 2 and 3, we calculated the velocities $U_i$ for the particles shown in Table 1. The results are given in Table 2. There are no known equations describing the terminal velocities of particles with densities between 300 and 900 kg/m$^3$ (beds No. 3, 4, 10 and 11). As a first approximation, these velocities were calculated using Eq. 10. The maximum difference between the experimental and the calculated values of $U_t$ using Eqs. 9 and 10 is 20% and the variation is 8%. Therefore, the difference in behavior of freely falling and rising single particles can explain the difference in performance of the upflow and inverse fluidized beds, respectively. The plot of $Re_t$ calculated from the experimental $U_i$ vs. $Re_t$ corresponding to the calculated values for $U_i$ is given in Figure 5. It can be seen that $Re_t$ calculated from the modified drag curve (Eqs. 9 and 10) are located around the diagonal of the plot and therefore they fit the experimental data better than $Re_t$ calculated from the standard drag curve (Eqs. 4 and 5). All the values for $Re_t$, and therefore terminal velocities, calculated from the standard drag curve are bigger than the experimental ones at $Re_t > 130$. When $Re_t < 130$, these values are close to each other. This can be explained by the fact that the original and modified drag curves are the same in this region of $Re_t$.

The theoretical curves of bed expansion calculated using the new values for $U_i$ (from Eqs. 2, 3, 9 and 10) and the Richardson-Zaki Eq. 1 are plotted in Figures 2-4 (the solid lines). A good agreement between the theoretical and experimental data was observed.

The standard deviations between the different correlations and the experimental data were calculated. The Richardson-

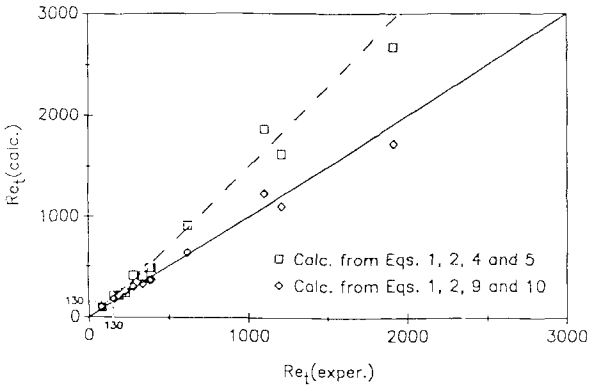


**Figure 5. Comparison between experimental and calculated $Re_t$**

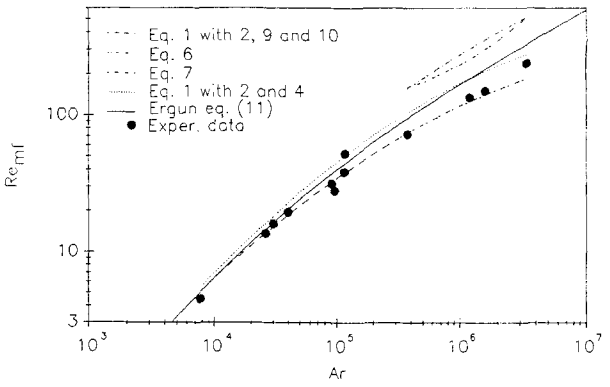


**Figure 6. Dependence between minimum fluidization *Re* and Archimedes number.**

Zaki correlation with $U_i$ calculated from the modified drag curve (Eqs. 9 and 10) fits the experimental data most closely, with a standard deviation 2.8 times smaller than that calculated using Eqs. 1, 2 and 4, 5.5 times smaller than that obtained from Eq. 7, and 6.7 times smaller than the standard deviation between the experimental data and those predicted from Eqs. 2, 4 and 6.

### *The minimum fluidization velocity*

It is interesting to compare the values of minimum fluidization velocities $U_{mf}$ of the inverse fluidized bed with those obtained from Eqs. 1, 6 and 7. The experimental values of $U_{mf}$ were determined from the intercept of the $ln\epsilon$-$lnU$ lines with the horizontal axis at $ln\epsilon = ln0.4$. A relation based on the Ergun equation was used for calculating the theoretical minimum fluidization velocity (Richardson, 1971):

$$Re_{mf} = 25.7(\sqrt{1 + 5.53 \times 10^{-5} Ar} - 1) \tag{11}$$

Theoretically, $U_{mf}$ should be the same for both upflow and inverse fluidization for the following reason. The Ergun equation is based on main assumption that the drag force of the fluid moving with a superficial velocity $U_{mf}$ is equal to the weight of the particles in the bed:

**Table 3. Minimum Fluidization Velocities Calculated from Different Models and Determined Experimentally**

| Bed No. | Exp. Results | Eq. 11 | Model 1, $U_t$ from Eq. 4 | Model 1, $U_t$ from Eqs. 9, 10 | Model 6 | Model 7 |
|---|---|---|---|---|---|---|
| 1 | 0.026 | 0.037 | 0.034 | 0.024 | 0.050 | 0.048 |
| 2 | 0.021 | 0.027 | 0.029 | 0.020 | 0.046 | 0.039 |
| 3 | 0.012 | 0.016 | 0.017 | 0.012 | — | — |
| 4 | 0.019 | 0.016 | 0.019 | 0.014 | — | — |
| 5 | 0.025 | 0.034 | 0.034 | 0.023 | 0.050 | 0.045 |
| 6 | 0.033 | 0.045 | 0.040 | 0.027 | 0.072 | 0.056 |
| 7 | 0.0087 | 0.0093 | 0.0089 | 0.0085 | — | — |
| 8 | 0.016 | 0.018 | 0.022 | 0.017 | — | — |
| 9 | 0.034 | 0.038 | 0.0042 | 0.0040 | — | — |
| 10 | 0.010 | 0.012 | 0.014 | 0.011 | — | — |
| 11 | 0.064 | 0.067 | 0.0080 | 0.0076 | — | — |
| 12 | 0.0045 | 0.0041 | 0.0055 | 0.0048 | — | — |

$$\frac{\Delta p}{H_o} = g(\rho_p - \rho_l)(1 - \epsilon_o) \tag{12}$$

In the bed containing light particles, the weight force should be replaced by the buoyancy force:

$$-\frac{\Delta p}{H_o} = g(\rho_l - \rho_p)(1 - \epsilon_o) \tag{13}$$

Since Eqs. 12 and 13 are identical, the minimum fluidization velocities in both upflow and inverse fluidized beds should be equal when parameters of the liquid phase, particle diameters and the absolute values of $(\rho_p - \rho_l)$ are equal.

The minimum fluidization velocities obtained from Eqs. 1, 6, 7, 11 and from the inverse fluidized bed experiments are compared in Table 3.

The dependence between the values of $Re_{mf}$ calculated from the minimum fluidization velocities given in Table 3 and the Archimedes numbers is plotted in Figure 6. It can be seen that the minimum fluidization velocities predicted by the Richardson and Zaki Eq. 1 with $U_i$ determined from the standard drag curve fit most closely those calculated from the Ergun equation in the entire region of $Ar$, while $U_{mf}$ calculated from Eqs. 6 and 7 exceed the theoretical values. The experimental minimum fluidization velocities and the ones obtained from the Richardson and Zaki equation with $U_i$ calculated from the modified drag curve approximate those predicted from the Ergun equation only when $Re_{mf} < 50$–$70$.

The difference between the theoretical and experimental values of $U_{mf}$ for the inverse fluidized bed at high Reynolds numbers could be explained by analysis of the behavior of two single spheres in a vertical liquid flow. One of them is placed on a grid (the density of this sphere is higher than that of the liquid) and the second one is below a grid (because $\rho_p < \rho_l$), and the liquid flows upwards and downwards, respectively. Both spheres have the same diameter and the same absolute values $(\rho_p - \rho_l)$. $Re_t$ of both spheres is much higher than 130. Let us assume that the grid has no effect on the liquid flow. The liquid velocity is increased starting from $U = 0$ and hence from $Re = 0$. The liquid flow around both spheres is viscous until $Re = 1$. As $Re$ is further increased up to 130, a stable wake formation is observed. Hence, in the region $0 < Re < 130$, the flow streamlines are axisymmetric (Clift et al., 1978). At

$Re > 130$, vortex shedding begins which induces periodic pulsations of the liquid around the sphere. This causes a destruction of the axial symmetry of the flow which results in an imbalance of the forces applied to the sphere in the horizontal direction.

The main force (along with that of viscosity) opposing to this horizontal force is the inertial one. The first (heavy) sphere is much more inert and its movement in the horizontal direction due to the imbalance of the horizontal forces will be insignificant. On the contrary, the lighter sphere with $\rho_p < \rho_l$ will fluctuate intensively because of its smaller mass and therefore, smaller inertia. Hence, the behavior of the heavy and the light spheres in a fluid with $Re < 130$ is the same, while at $Re > 130$ it is different and this difference increases as $|\rho_p - \rho_l|$, and hence $Re$, increases. This critical value of $Re$ should be lower than 130 in a bed of particles because of the more intensive liquid turbulence. The data in Figure 6 show that the critical Reynolds number is around 50–70. The intensive, high-frequency fluctuation of low-density particles in inverse fluidized bed has been previously observed (Karamanev, 1988).

The mechanism proposed above can explain the fact that an inverse fluidized bed consisting of low-density particles has smaller $U_{mf}$ compared to that of an upflow fluidized bed (and that predicted by the Ergun equation) for $Re_{mf} > 50$–70. This difference is negligible when $Re_{mf}$ is less than the critical one.

## Notation

$Ar$ = Archimedes number defined by $d^3 g(\rho_p - \rho_l)\rho_l/\mu^2$ when $\rho_p > \rho_l$ and by $d^3 g(\rho_l - \rho_p)\rho_l/\mu^2$ when $\rho_p < \rho_l$
$C_D$ = particle drag coefficient
$d$ = particle diameter
$D$ = column diameter
$f$ = drag function for multiparticle system
$g$ = gravity acceleration
$H_o$ = height of the fixed bed
$n$ = exponent in Eqs. 1 and 6
$N_D$ = Best number defined by Eq. 5
$Re$ = Reynolds number defined by $dU\rho_l/\mu$
$Re_{mf}$ = minimum fluidization Reynolds number defined by $dU_{mf}\rho_l/\mu$
$Re_t$ = particle Reynolds number defined by $dU_t\rho_l/\mu$
$U$ = superficial liquid velocity
$U_i$ = the extrapolated value of $U$ as $\epsilon$ approaches 1
$U_{mf}$ = minimal fluidization velocity
$U_t$ = terminal velocity of solid particle

### *Greek letters*

$\epsilon$ = bed porosity
$\epsilon_o$ = porosity of a fixed bed of particles
$\mu$ = liquid viscosity
$\rho_l$ = liquid density
$\rho_p$ = particle density

## Literature Cited


Atkinson, B., *Biological Fluidized Bed Treatment of Water and Wastewater*, P. F. Cooper and B. Atkinson, eds., E. Horwood, Chichester, U.K. (1981).

Chavarie, C., D. Karamanev, L. Nikolov, and J. Champagne, "Simulation d'un Reacteur a Biofilm a Fluidisation Inversee," *La Fluidisation*, 254 (1986).

Chavarie, C., and D. Karamanev, "Use of Inverse Fluidization in Biofilm Reactors," *Int. Symp. on Bioreactor Fluid Dynamics*, Cambridge, U.K., 181 (May 15–17, 1986).

Clift, R., J. R. Grace, and M. E. Weber, *Bubbles, Drops and Particles*, Academic Press, New York (1978).

Denn, M. M., *Process Fluid Mechanics*, Prentice-Hall, Englewood Cliffs, NJ (1980).

Dion, N., J. Goulet, and P. Boyaval, "Milk Protein Hydrolysis in a Inverse Fluidized Bed Biofilm Reactor with *L. helveticus* Cells Immobilized in Polystyrene Balls," *Abstr. Int. Biotechnol. Symp.*, Paris, France, 271 (July 17–22, 1988).

Endo, I., T. Nagamune, K. Tachi, and T. Kobayashi, "Fluidized Bed Bioreactor: Antibiotic Production," *Abstr. Int. Biotechnol. Symp.*, Paris, France, 37 (July 17–22, 1988).

Fan, L.-S., K. Muroyama, and S.-H. Chern, "Hydrodynamic Characteristics of Inverse Fluidization in Liquid-Solid and Gas-Liquid-Solid Systems," *Chem. Eng. J.*, **24**, 143 (1982).

Garnier, A., C. Chavarie, G. Andre, and D. Klvana, "The Inverse Fluidization Airlift Bioreactor: 1. Hydrodynamic Studies," *Chem. Eng. Commun.*, **98**, 31 (1990).

Holladay, D. W., et al., "Biodegradation of Phenolic Waste Liquors in Stirred Tank, Columnar and Fluidized Bed Bioreactors," *AIChE Symp. Ser.*, **74**(172), 241 (1978).

Jeris, J. S., R. W. Owens, and F. Flood, "Secondary Treatment of Municipal Wastewater with Fluidized Bed Technology," *Biological Fluidized Bed Treatment of Water and Wastewater*, P. F. Cooper and B. Atkinson, eds., 112, E. Horwood, Chichester, U.K. (1981).

Jewell, W. J., M. S. Switzenbaum, and J. W. Morris, "Municipal Wastewater Treatment with the Anaerobic Attached Microbial Film Expanded Bed Process," *J. Water Poll. Control Fed.*, **53**, 482 (1981).

Karamanev, D. G., and L. N. Nikolov, "Influence of Some Physicochemical Parameters on Bacterial Activity of Biofilm," *Biotechnol. Bioeng.*, **31**, 295 (1988).

Karamanev, D. G., and L. N. Nikolov, "Free Rising Spheres Do Not Obey Newton's Law for Free Settling," *AIChE J.*, **38**, 1843 (1992).

Karamanev, D. G., "Modelling, Design and Scale-up of Inverse Fluidized Bed Biofilm Reactor," PhD Thesis, Bulgarian Academy of Sciences (1988).

Livingston, A. G., and H. A. Chase, "Modelling Phenol Degradation in a Fluidized-Bed Bioreactor," *AIChE J.*, **35**, 1980 (1989).

Muroyama, K., and L.-S. Fan, "Fundamentals of Gas-Liquid-Solid Fluidization," *AIChE J.*, **31**, 1 (1985).

Nikolov, L., D. Karamanev, and D. Elenkov, "Biofilm Reactor with Mobile Bed," Bulgarian Patent 32,910 (Sept. 21, 1981).

Nikolov, L., and D. Karamanev, "Experimental Study of Inverse Fluidized Bed Biofilm Reactor," *Can. J. Chem. Eng.*, **65**, 214 (1987).

Nikolov, L., and D. Karamanev, "The Inverse Fluidized Bed Biofilm Reactor: A New Laboratory Scale Apparatus for Biofilm Research," *J. Ferm. Bioeng.*, **69**, 265 (1990).

Nikolov, L., and D. Karamanev, "The Inverse Fluidization—A New Approach for Biofilm Reactor Design," *Studies Environ. Sci.*, **42**, 177 (1991).

Nikolov, L., D. Karamanev, T. Penev, and D. Dimitrov, "Full-Scale Inverse Fluidized Bed Biofilm Reactor for Wastewater Treatment," *2nd Int. Biotechnol. Conf.: Asian-Pacific Biotechnol. Conf.*, 112, Seoul, Korea (May 6–9, 1990).

Nikov, I., and D. Karamanev, "Liquid-Solid Mass Transfer in Inverse Fluidized Bed," *AIChE J.*, **37**, 781 (1991).

Oh, D. K., C. K. Hyun, J. H. Kim, and Y. H. Park, "Production of Penicillin in a Fluidized Bed Bioreactor," *Biotechnol. Bioeng.*, **32**, 569 (1988).

Ramamurthy, K., and K. Subbaraju, "Bed Expansion Characteristics of Annular Liquid-Fluidized Beds," *Ind. Eng. Chem. Process Des. Dev.*, **12**, 184 (1973).

Riba, J. P., and J. P. Couderc, "Expansion de Couches Fluidisees par des Liquides," *Can. J. Chem. Eng.*, **55**, 118 (1977).

Richardson, J. F., "Transient Fluidization and Particulate Systems," *Fluidization*, J. F. Davidson and D. Harrison, eds., 39, Academic Press, New York (1971).

Richardson, J. F., and W. N. Zaki, "Sedimentation and Fluidization," *Trans. Inst. Chem. Eng.*, **32**, 35 (1954).

Shugerl, K., "Biofluidization: Application of the Fluidization Technique in Biotechnology," *Can. J. Chem. Eng.*, **67**, 178 (1989).

Tang, W. T., and L.-S. Fan, "Steady-State Phenol Degradation in a Draft-Tube, Gas-Liquid-Solid Fluidized-Bed Bioreactor," *AIChE J.*, **33**, 239 (1987).

Wen, C. Y., and Y. H. Yu, "Mechanics of Fluidization," *Chem. Eng. Progr. Symp. Ser.*, **62**, 100 (1966).


*Manuscript received Sept. 23, 1991, and revision received June 8, 1992.*